




LA-ICP-MS U-Pb zircon dating of rocks of the Jacareacanga Group, Tapajós Domain, Amazon Craton, Brazil

Jenny Alexandra Ortega Cardozo^{1*} , Marcelo Vasquez² , Marco Antonio Galarza Toro¹ 

Abstract

The Jacareacanga Group comprises mafic to ultramafic schists, metacherts, quartzites, pelitic paragneisses, and amphibolites related to siliciclastic-chemical sedimentation and mafic-ultramafic volcanism. These rocks of the Jacareacanga Group correspond to turbidite-related sediments and oceanic crust basalts of a back-arc or trench basin of the early magmatic Cuiú-Cuiú Arc of the Tapajós Domain in the Amazon Craton. Field data and petrographic analysis support the new zircon U-Pb ages obtained through LA-ICP-MS for the rocks of the Jacareacanga Group. A $\pm 10\%$ concordance criterion applied, along with an exclusion of ages < 2000 Ma to mitigate interference from later events, such as granitic intrusions. Two pelitic paragneisses yielded $^{207}\text{Pb}/^{206}\text{Pb}$ ages between 2008 and 2042 Ma and mica schist ages of ca. 2056 Ma, considered to be the maximum sedimentation age of the protoliths of metasedimentary rocks. Zircon populations from the Rhyacian to the Mesoarchean indicate provenance from adjacent cratonic areas. This study shows that the Jacareacanga Basin was formed during the early Orosirian. The oldest detrital zircon ages support provenance from a magmatic arc basin of a continental margin comprising Rhyacian to Mesoarchean crust.

KEYWORDS: Tapajós Domain; Jacareacanga Group; Cuiú-Cuiú Arc; LA-ICP-MS U-Pb zircon dating.

1 INTRODUCTION

The Tapajós Domain is located in the central part of the Amazon Craton (Fig. 1) and is related to the accretion of one (Tassinari, 1996; Tassinari & Macambira, 1999, 2004) or more magmatic arcs (Santos et al., 2000, 2001, 2004) onto an Archean continent during the Orosirian period.

The Jacareacanga Group consists of metavolcano-sedimentary rocks, with subordinate pelitic paragneisses and

amphibolites, whose sedimentation and volcanism are related to the formation of basins associated with the early Cuiú-Cuiú Magmatic Arc (2040-1998 Ma) of the Tapajós Domain (Santos et al., 2004).

The amount of zircon crystals necessary to investigate the provenance of detrital zircon populations and constrain the maximum sedimentation ages varies across the literature. Most researchers recommend more than 100 crystals (Andersen, 2005; Vermeesch, 2004). They also recommend the application of geochronological methods that allow dating large quantities at low cost and in a short time. Therefore, *in situ* dating methods, such as U-Pb dating via LA-ICP-MS, have become widely adopted for such purposes (Gehrels, 2014; Von Eynatten & Dunkl, 2012). Previous studies involving the Jacareacanga Group schists assumed these rocks to be para-derived. Santos et al. (2000) dated only four zircon crystals using TIMS. In turn, Almeida et al. (2001b) dated ten zircon grains using the Pb-evaporation method. Unfortunately, both studies employed inadequate methods and insufficient quantities of zircon crystals. Vasquez et al. (2019) applied the U-Pb dating method by LA-ICP-MS on zircon crystals from pelitic paragneisses of this unit, but the sample size (< 100 crystals) was not sufficient for comprehensive analysis.

This study presents robust LA-ICP-MS U-Pb data for zircon crystals from a mica schist and two pelitic paragneisses of the Jacareacanga Group. More than 100 crystals were analyzed for each rock type (117 crystals from FH-27, 116 crystals from FH-21, and 163 crystals from MV-58A and 58C), supplemented by data from Vasquez et al. (2019). The application of the $\pm 10\%$ concordance criterion to these larger

Supplementary file:

Supplementary data associated with this article can be found in the online version: <https://doi.org/10.48331/scielodata.SHYME4>.

Supplementary File 1. LA-ICP-MS U-Pb isotopic data for pelitic paragneiss FH-27.

Supplementary File 2. LA-ICP-MS U-Pb isotopic data for sample FH-27, taken from Vasquez et al. (2019).

Supplementary File 3. LA-ICP-MS U-Pb isotopic data for pelitic paragneiss FH-21.

Supplementary File 4. LA-ICP-MS U-Pb isotopic data for sample FH-21, taken from Vasquez et al. (2019).

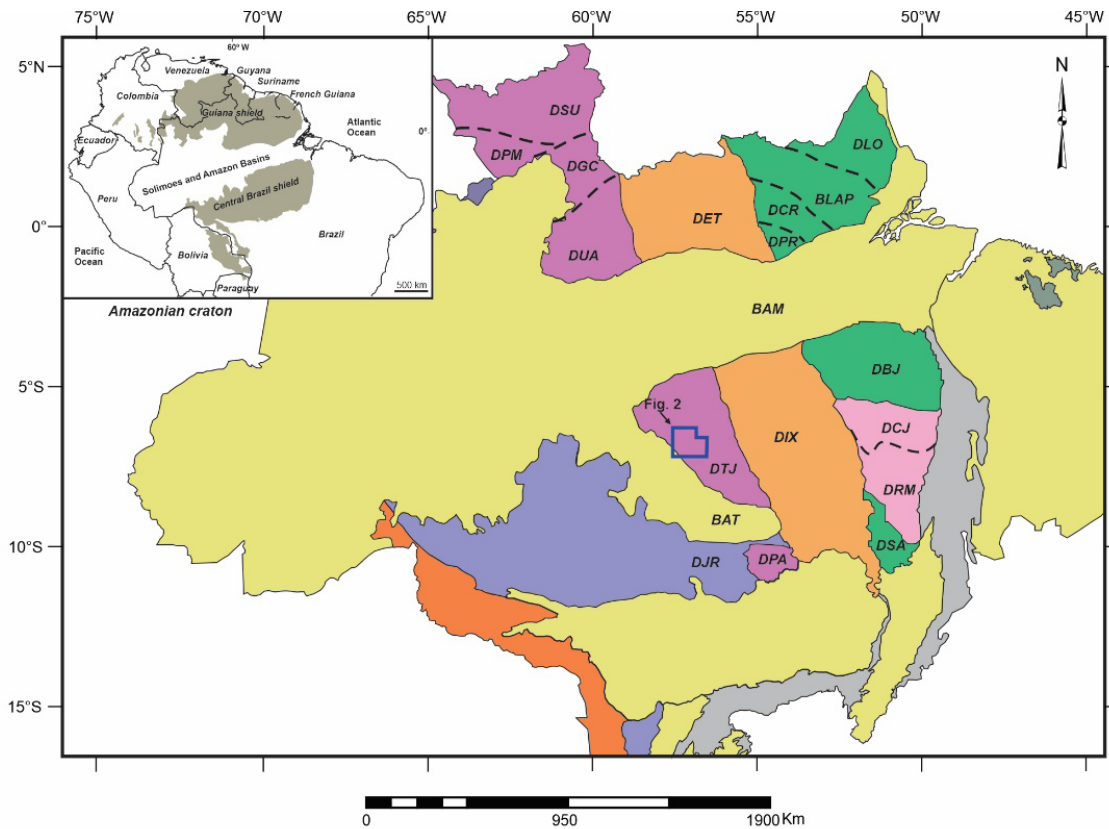
Supplementary File 5. LA-ICP-MS U-Pb isotopic data for sample MV-58A and MV-58C.

¹Universidade Federal do Pará, Instituto de Geociências, Programa de Pós-graduação em Geologia e Geoquímica – Belém (PA), Brazil. E-mail: jenny.9525@hotmail.com; antogt@ufpa.br

²Serviço Geológico do Brasil – Belém (PA), Brazil. E-mail: marcelo.vasquez@sgb.gov.br

*Corresponding author.





Tectonic Provinces

- | | |
|---|----------------------------------|
| Tocantins (Araguaia and Paraguay belts) | Phanerozoic basins and covers |
| Parnaíba (São Luís cratonic fragment and Gurupi belt) | <i>BAM</i> - Amazon Basin |
| | <i>BAT</i> - Upper Tapajós Basin |

Provinces of the Amazon Craton

- | | |
|--|------------------------------------|
| | Sunsás (1450 - 1000 Ma) |
| | Rio Negro (1820 - 1520 Ma) |
| | Rondônia-Juruena (1850 - 1540 Ma) |
| | Central Amazonian (1990 - 1860 Ma) |
| | Tapajós-Parima (2030 - 1860 Ma) |
| | Transamazonas (2260 - 2060 Ma) |
| | Carajás (3000 - 2500 Ma) |

Tectonic domains

- | | |
|---|--|
| <i>DRM</i> - Rio Maria domain | <i>DIX</i> - Iriri-Xingu domain |
| <i>DCJ</i> - Carajás domain | <i>DTJ</i> - Tapajós domain |
| <i>BLAP</i> - Amapá block domain | <i>DPA</i> - Peixoto de Azevedo domain |
| <i>DCR</i> - Carecuru domain | <i>DUA</i> - Uatumã-Anauá domain |
| <i>DPR</i> - Paru domain | <i>DPM</i> - Parima domain |
| <i>DLO</i> - Loreço domain | <i>DSU</i> - Surumu domain |
| <i>DBJ</i> - Bacajá domain | <i>DCG</i> - Central Guinea domain |
| <i>DSA</i> - Santana do Araguaia domain | <i>DJU</i> - Juruena domain |
| <i>DET</i> - Erepecuru-Trombetas domain | |



Figure 1. Map of the geochronological provinces of the Amazon Craton and the tectonic domains of Santos (2003) of the eastern part (modified after Vasquez et al., 2008), with the location of the study area.

datasets provided more robust zircon populations. The U-Pb zircon ages allowed the identification of the main detrital zircon populations and helped constrain the sedimentation age of the Jacareacanga Basin, identified as the oldest basin of the Cuiú-Cuiú Arc.

2 REGIONAL TECTONIC CONTEXT

The Tapajós Domain corresponds to the central part of the Tapajós-Parima Province of the Amazon Craton (Fig. 1). This province, also referred to as Ventuari-Tapajós Province,

has been associated with the accretion of one (Tassinari, 1996; Tassinari & Macambira, 1999, 2004) or more magmatic arcs (Santos et al., 2000, 2001, 2004) onto an Archean continent.

The Geological Survey of Brazil has mapped the Tapajós Domain since the 1970s (Almeida et al., 2000; Bahia & Quadros, 2000; Bizinella et al., 1980; Ferreira et al., 2000; Guimarães et al., 2015; Klein & Vasquez, 2000; Klein et al., 2001; Melo et al., 1980; Pessoa et al., 1977; Vasquez & Klein, 2000; Vasquez et al., 2017). This tectonic domain hosts important gold deposits and subordinate cassiterite (Sn), columbite (Nb-Ta), and diamond (Coutinho, 2008; Guimarães

et al., 2015; Klein et al., 2001; Vasquez et al., 2017) deposits, which is why it is also called Tapajós Mineral Province or Tapajós Gold Province.

The geochronological database for igneous rocks of the Tapajós Domain encompasses U-Pb ages from zircon, titanite, and baddeleyite, as well as Pb-Pb ages from zircon, ranging from 2033 ± 7 to 1864 ± 18 Ma, with subordinated ages of 1786 ± 14 , 1780 ± 7 , and 1186 ± 12 Ma, as compiled by Vasquez et al. (2017). Sm-Nd data for the igneous rocks from 2020 to 1981 Ma include $\epsilon\text{Nd}(t)$ values from -0.59 to -3.71 and Sm/Nd- T_{DM} ages from 2.26 to 2.49 Ga (Lamarão et al., 2005; Vasquez et al., 2017). Local granitoids yielding $\epsilon\text{Nd}(t)$ of +2.6 and +1.8 with Sm/Nd- T_{DM} ages of 2.16 to 2.09 Ga and $\epsilon\text{Nd}(t)$ of -1.49 and -5.45 with Sm/Nd- T_{DM} ages of 2.58 to 2.41 Ga (Sato & Tassinari, 1997) indicate a Paleoproterozoic juvenile accretion with few interactions with the Archean crust. This Nd-isotope signature is also present in igneous rocks from 1907 to 1864 Ma, as compiled by Vasquez et al. (2017). These two Paleoproterozoic juvenile accretions would be related to early Cuiú-Cuiú and late Tropas magmatic arcs of the Tapajós Domain, respectively (Lamarão et al., 2005; Vasquez et al., 2017).

The calc-alkaline granitoids of the Cuiú-Cuiú Complex (Coutinho et al., 2008; Santos et al., 2004; Vasquez et al., 2002, 2017) and felsic volcanic and pyroclastic rocks of the Comandante Arara Formation (Vasquez et al., 2017) were succeeded by high-K calc-alkaline to shoshonitic felsic volcanic and pyroclastic rocks of the Vila Riozinho Formation (Guimarães et al., 2015; Lamarão et al., 2002; Vasquez et al., 2017). Calc-alkaline rocks from 2033 to 1996 Ma were related to the early stages of the Cuiú-Cuiú Arc, while high-K calc-alkaline to shoshonitic granitoids from 1989 to 1955 Ma of the Creporizão Suite (Borgo et al., 2017; Cassini et al., 2020; Lamarão et al., 2002) could be related to the late stages of the Cuiú-Cuiú Arc. However, these high-K calc-alkaline granitoids have also been related to a transcurrent post-collisional setting (Vasquez et al., 2002, 2017). Additionally, the calc-alkaline granitoids of the Tropas and Parauari suites, along with felsic volcanic and pyroclastic rocks of the Salustiano Formation, high-K calc-alkaline intermediate volcanic and pyroclastic rocks of the Bom Jardim Formation, and gabbros of the Ingarana Suite emplaced between 1907 and 1870 Ma, were related to the Tropas Arc (Coutinho et al., 2008; Santos et al., 2004; Vasquez et al., 2002, 2017). Coeval alkaline granites and felsic volcanic and pyroclastic rocks of the Moraes Almeida Formation (Lamarão et al., 2002; Vasquez et al., 2002, 2017) could be related to a post-orogenic extension (Fig. 2).

3 JACAREACANGA GROUP

The Jacareacanga Group is located in the southwestern portion of the Tapajós Domain (Fig. 1). These rocks crop out as belts of supracrustal rocks elongated in the NW-SE to NNW-SSE direction (Ferreira et al., 2000).

The Jacareacanga Group was divided into the Sai Cinza and Cadiriri Formations (Vasquez et al., 2019, 2020) (Fig. 2).

The Sai Cinza Formation is composed of muscovite, biotite, chlorite, and actinolite schists, along with ferruginous metacherts. Locally, tremolite and talc schists, meta-greywackes, and amphibolites also crop out (Ferreira et al., 2000; Melo et al., 1980; Vasquez et al., 2019, 2020). The Cadiriri Formation corresponds to quartzite lenses oriented in the NNW direction, in agreement with the foliated rocks of the Sai Cinza Formation (Ferreira et al., 2000; Vasquez et al., 2019, 2020). This formation is a volcano-sedimentary sequence composed of siliciclastic and chemical sediments related to platform sedimentation with associated basic seafloor volcanism (Ferreira et al., 2000). However, Santos et al. (2000) interpreted it as turbidite sedimentation and basic volcanism occurring in either an arc-trench basin or a magmatic back-arc basin.

The volcano-sedimentary sequence of the Jacareacanga Group underwent a regional low- to medium-grade metamorphism, from the greenschist to the epidote amphibolite facies (Melo et al., 1980). Locally, this sequence attained very low-grade metamorphism conditions, resulting in meta-greywackes (Ferreira et al., 2000). High-grade metamorphism is marked by the metamorphic paragenesis (sillimanite-cordierite-garnet-biotite) observed in the pelitic paragneisses (Figs. 3 and 4), with neosome development marked by veins of garnet-muscovite granite/peraluminous leucogranite, indicating anatexis at ca. 1960 Ma (Vasquez et al., 2019). This wide range of metamorphic conditions is likely associated with progressive regional metamorphism related to the accretion of Cuiú-Cuiú magmatic arc. However, detailed studies supporting this interpretation are currently lacking.

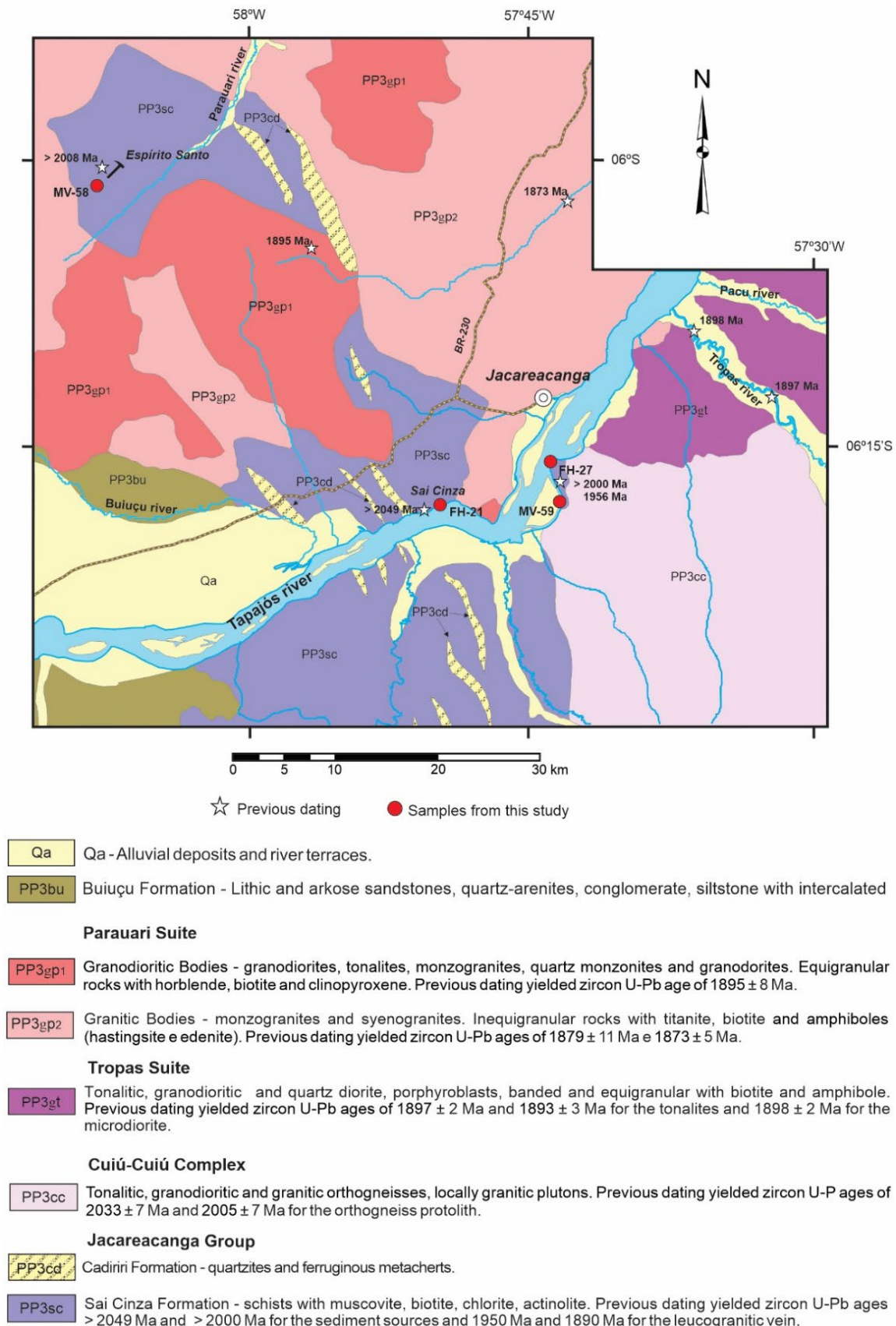
Ductile deformation is marked by schistosity (Fig. 5), compositional banding (Fig. 3), boudinage of quartzite lenses, and tight folds initially with NNW-SSE orientation (Fig. 4). The ductile foliations were transported by mylonitic foliation and crenulation cleavage trending NW-SE (Almeida et al., 2001a, Santos & Coutinho, 2008; Vasquez et al., 2019). Intrusions of lenses of peraluminous leucogranites bearing biotite, muscovite, and garnet (neosome) occurred within the pelitic paragneisses (Fig. 3).

Xenoliths of pelitic paragneisses, amphibolite, and schists from the Jacareacanga Group are hosted within the granitoids and orthogneisses of the Cuiú-Cuiú Complex, indicating the intrusive relationship. Furthermore, batholiths of tonalites, granodiorites, and granites of the Parauari and Tropas Suites (1900 - 1870 Ma) cut the rocks of the Jacareacanga Group (Fig. 2).

Santos et al. (2000) obtained TIMS U-Pb zircon ages around 2100 Ma for a schist of the Sai Cinza Formation. In turn, Almeida et al. (2001b) obtained zircon ages between 2034 and 2008 Ma using the Pb-evaporation method. The number of dated zircon crystals and the methods applied were not appropriate to determine the age of the zircon sources and the maximum sedimentation age of the metasedimentary rocks. The researchers recommend more than 100 crystals, and the application of geochronological methods that allow dating large quantities of crystals (Andersen, 2005; Vermeesch, 2004). Furthermore, Vasquez et al. (2019) dated zircon grains from the pelitic paragneisses and peraluminous leucogranite veins

by LA-ICP-MS and determined sedimentation ages of 2049 and 2000 Ma for the protoliths of the paragneisses, and age of 1956 ± 27 Ma for the neosome of peraluminous leucogranitic veins. Zircon populations of ca. 1950 and 1890 Ma were related

to the granitic rocks that crosscut the paragneisses. Thus, the younger zircon population was correlated with the intrusions of the Parauari Suite granitoids (1895 and 1873 Ma) that cross-cut the Jacareacanga Group (Fig. 2).



Source: modified after Vasquez et al. (2020).

Figure 2. Simplified geological map of the Jacareacanga area, with the location of the dated samples and samples selected for this study.

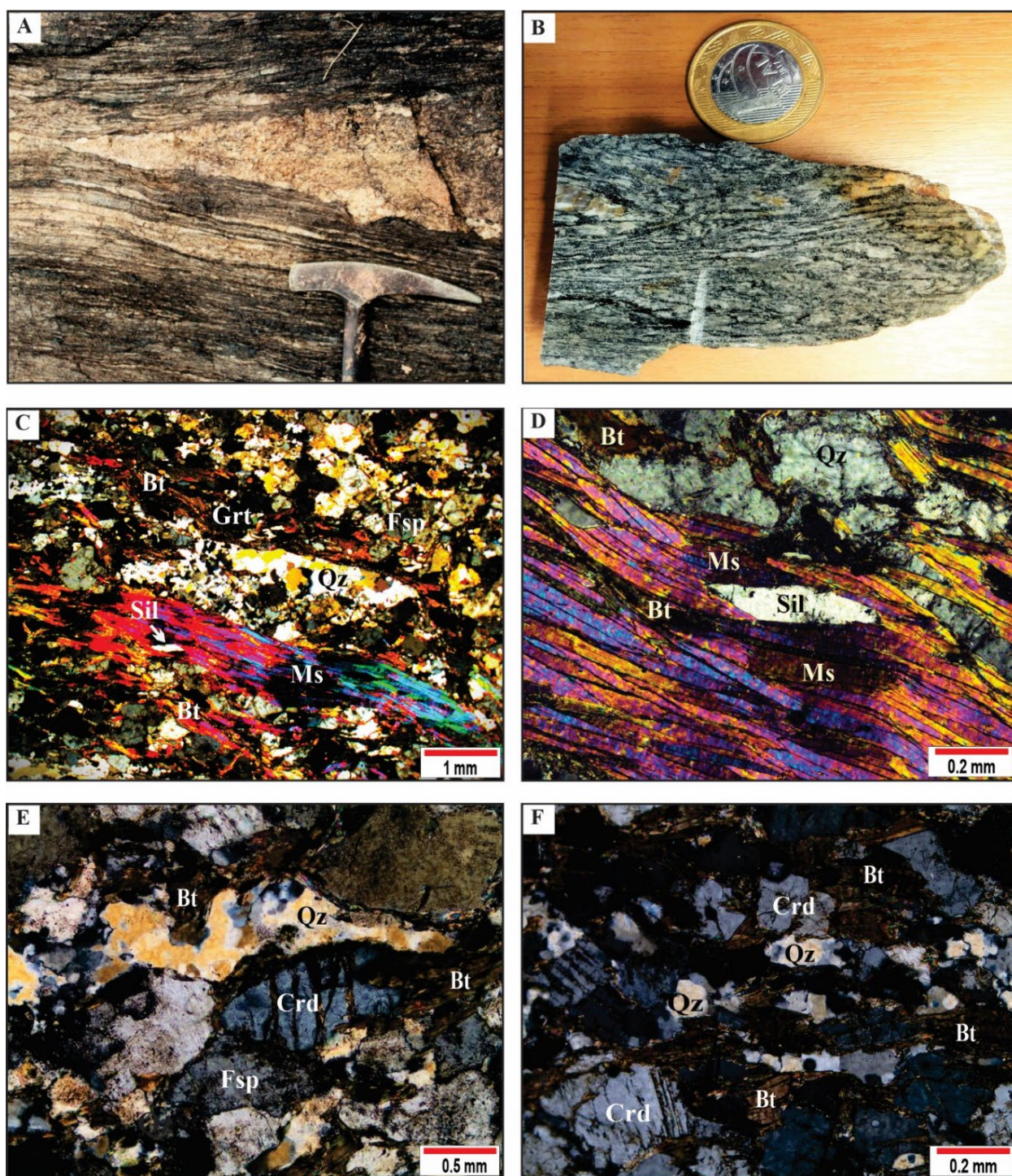


Figure 3. Structures and textures of the pelitic paragneiss FH-27: (A) Gneissic banding with concordant mm- to cm-thick leucogranitic lenses; (B) Gneissic banding composed of felsic and mafic bands alternating with mm- to cm-thick granitic lenses; (C) Granoblastic bands of quartz (Qz) and feldspars (Fsp) with garnet porphyroblasts (Grt) and lepidoblastic bands of muscovite (Ms) with biotite (Bt) and sillimanite (Sil); (D) Detail of lamellar sillimanite and muscovite with interspersed biotite; (E) Cordierite porphyroblast (Crd) in granoblastic quartz and feldspar band; (F) Cordierite porphyroblast in a granolepidoblastic band with biotite. Photomicrographs taken in polarized light.

4 PROCEDURES AND METHODS

4.1 Sample preparation

Heavy mineral separations were carried out at the Mineral Analysis Laboratory of the SGB Branch Office in Belém (LAMIN-BE). The rocks were crushed and sieved, and the heavy minerals of the 0.250 to 0.180 mm grain-size fraction were concentrated by gravity methods in aqueous and dense

liquids (bromoform). It was refined by magnetic separation with ferrite and neodymium magnets, followed by isodynamic separation in a Frantz-type magnetic separator.

The zircon crystals were selected under a stereomicroscope, mounted in epoxy resin (mounts), and subsequently ground and polished in the facilities of the Institute of Geosciences of the Universidade Federal de Pará (IG-UFPA). The polished mounts were covered with an approximately 5 µm-thick gold

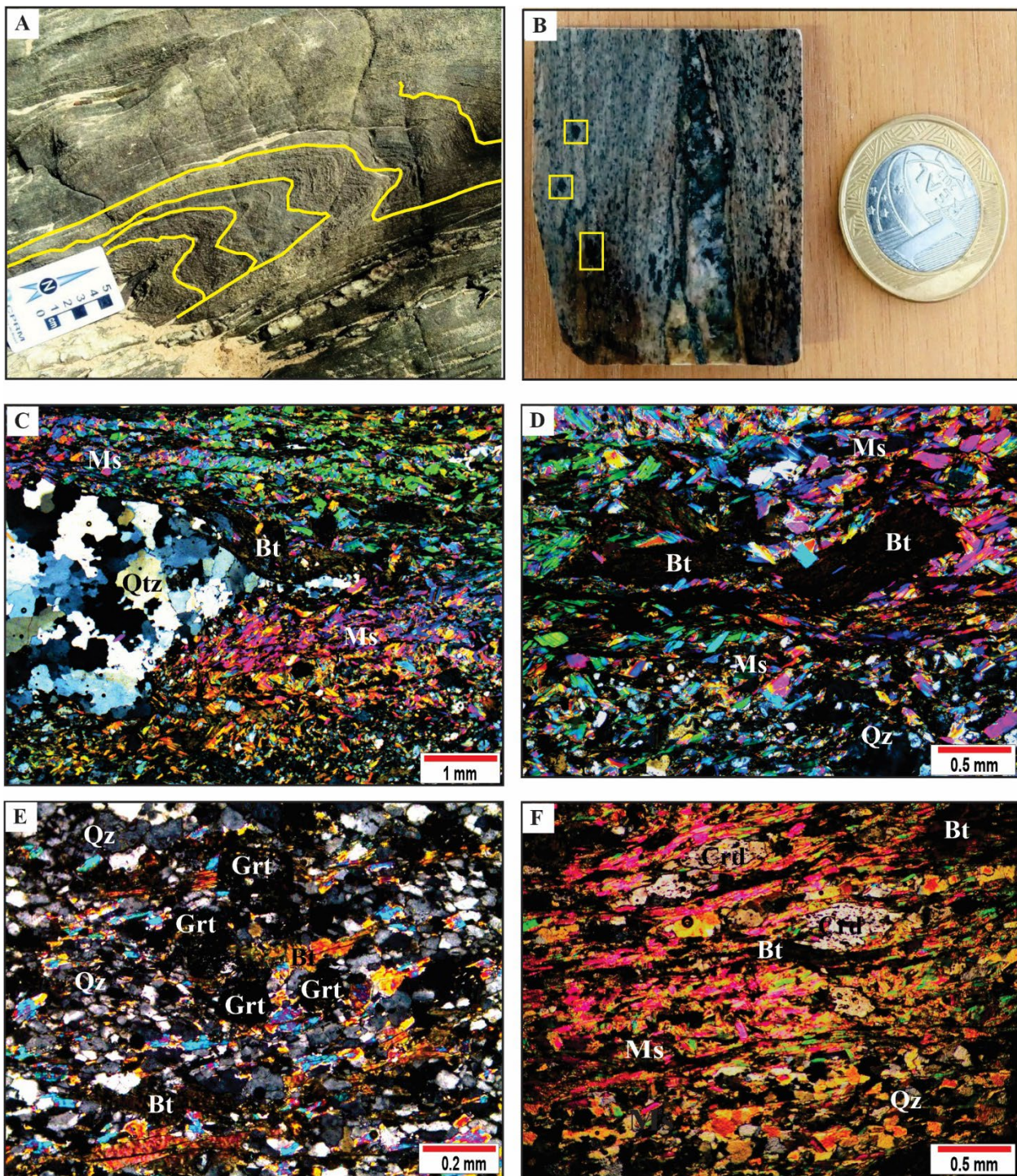


Figure 4. Structures and textures of the pelitic paragneiss FH-21: (A) Gneissic banding with tight folds and boudinated quartz veins; (B) Biotite porphyroblasts and granitic lenses concordant with banding; (C) Granolepidoblastic bands of muscovite (Ms), biotite porphyroblasts (Bt) and granoblastic quartz lens (Qz); (D) Detail of rotated biotite porphyroblasts; (E) Garnet porphyroblast (Grt) in a granolepidoblastic band; (F) Cordierite porphyroblast (Crd) in a granolepidoblastic band. Photomicrographs taken in polarized light.

film. Images of the zircon grains were obtained by a cathodoluminescence (CL) detector attached to a scanning electron microscope (SEM) at LAMIN-BE.

4.2 Cathodoluminescence images

CL images were used to select locations on zircon crystals free from fractures, mineral inclusions, and post-crystallization changes. These CL images revealed oscillatory zoning (igneous texture) in zircon crystals, core and edge structures related to

inherited core resorption, and mantle overgrowth by metamorphic recrystallization. Additional features included erasure of igneous zoning, dissolution of crystal edges, and metamict structures. Thus, the external morphology and internal textures of the crystals helped identify different zircon populations.

4.3 Analytical procedures

U-Pb zircon dating by LA-ICP-MS was performed at the Laboratory of Isotopic Geology of the Universidade Federal

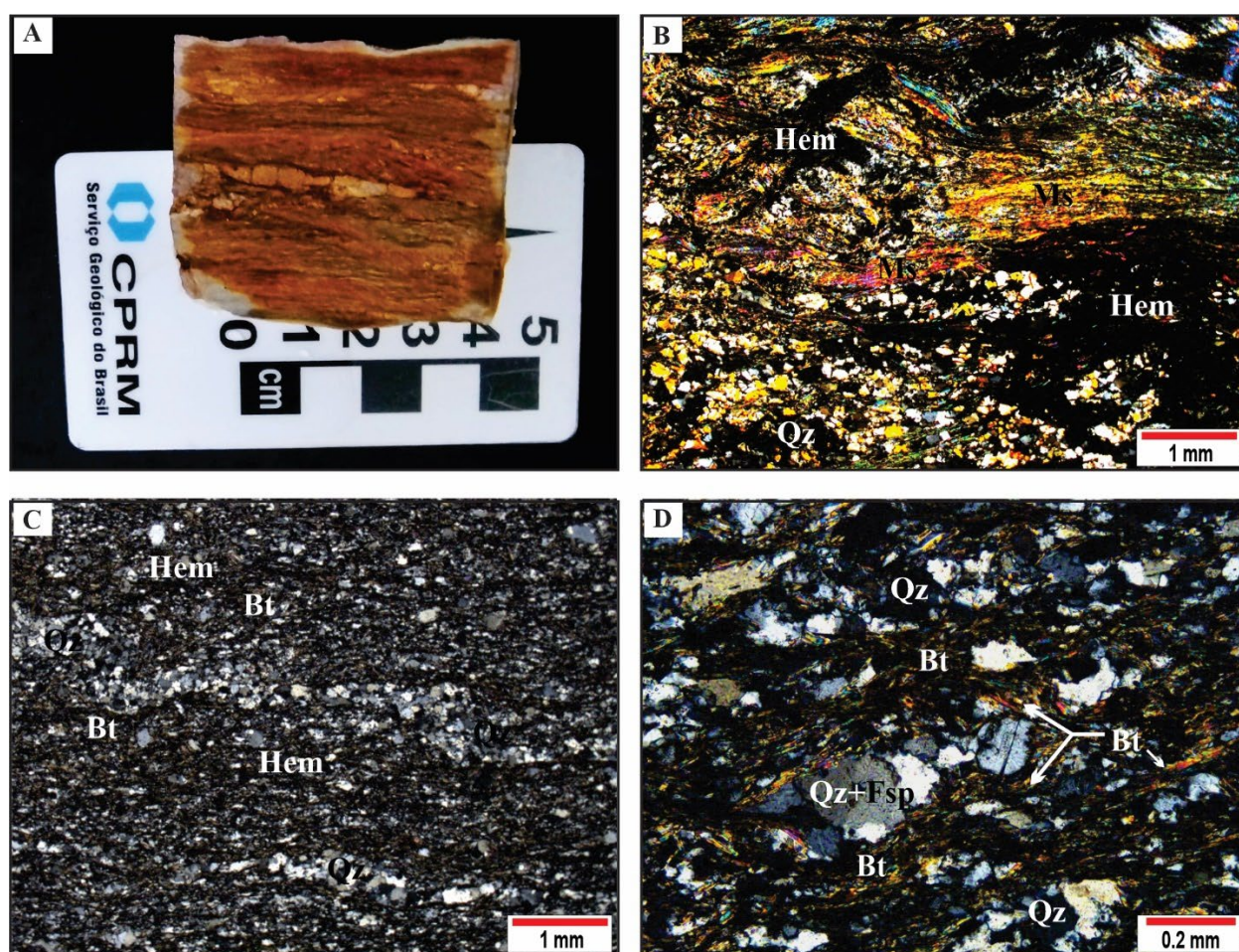


Figure 5. Structures and textures of MV-58A and quartz-mica schist MV-58C: (A) Pink gray and ocher saprolite of mica schists showing quartz venules along the schistosity; (B) Lepidoblastic layer of muscovite (Ms) in sample MV-58A and granoblastic layer of quartz (Qz) and opaque (iron hydroxide) minerals; (C) Granoblastic texture with quartz clasts, subordinate layers of biotite (Bt) and opaque minerals in sample MV-58C; (D) Detail of sigmoidal quartz and feldspar (Fsp) clasts surrounded by biotite in sample MV-58C. Photomicrographs taken in polarized light.

de Pará (Para-Iso) using a Thermo Finnigan high-resolution inductively coupled plasma source mass spectrometer equipped with a Neptune multi-collector and coupled, equipped with an Nd YAG 213 nm LSX-213 G2 CETAC laser ablation microprobe. The protocol and equipment configuration were applied according to Milhomem Neto et al. (2017). Analytical readings on samples were intercalated with standards to ensure accuracy and analytical control to avoid laser-induced elemental fractionation and instrumental mass discrimination. The zircon standards used were GJ-1 of 608.5 ± 1.5 Ma of age (Jackson et al., 2004) and Blue Berry (BB) of 562 ± 9 Ma of age (Santos et al., 2017).

Rare U, Pb, and Th isotopic data were reduced and corrected using a macro-enabled Microsoft Excel spreadsheet adapted by Chemale Jr. et al. (2012). Ages were calculated and isotopic results were plotted on concordia diagrams using the Isoplot/Ex software by Ludwig (2012). To calculate zircon U-Pb ages, data with $^{206}\text{Pb}/^{204}\text{Pb}$ ratios below 2500 were excluded from the age calculation to minimize the uncertainties resulting from common Pb correction. In this study, the ages provided from $^{207}\text{Pb}/^{206}\text{Pb}$ ratios were adopted and plotted with $100\% \pm 10\%$ concordance, which were considered the most representative ages of the

grains in frequency distribution graphs and relative probability curves.

When treating the results, a cutoff age of 2000 Ma was adopted as, according to Vasquez et al. (2019), ages below this threshold are related to metamorphic and magmatic events younger than the formation of the Jacareacanga Group (e.g., tonalites to granites of the Tropas and Paraguarí Suites - 1900-1870 Ma and Creporizão Suite - 1990-1960 Ma). This criterion was based on field and petrographic features that indicate granitic intrusion and anatexis of the Jacareacanga Group paragneisses, as identified by Vasquez et al. (2019). In addition, a more rigorous treatment was carried out using only grains of $^{207}\text{Pb}/^{235}\text{U}$, $^{206}\text{Pb}/^{238}\text{U}$, and $^{207}\text{Pb}/^{206}\text{Pb}$ ages that overlapped the limits of analytical errors. This step reduced the dataset to $100\% \pm 2\%$ concordance, with $^{207}\text{Pb}/^{206}\text{Pb}$ ages regarded as the most representative of the zircon populations analyzed in this study.

5 RESULTS PETROGRAPHY

Samples from two pelitic paragneisses (FH-21 and FH-27), two muscovite schists (MV-58A and MV-58C), and an amphibolite (MV-59) were collected during the mapping campaigns

sponsored by the Crustal Evolution and Metallogenes of the Tapajós Mineral Province Project (Vasquez et al., 2020).

5.1 Pelitic paragneisses

The pelitic paragneisses of the Jacareacanga Group crop out in the Sai Cinza indigenous area along the bank of the Tapajós River near Jacareacanga downtown (Fig. 2). Earlier mapping projects did not classify these rocks as paragneisses of the Jacareacanga Group — only Vasquez et al. (2019) correlated them to this unit.

The pelitic paragneiss of the FH-27 outcrop is a foliated, medium-grained gray gneiss displaying felsic bands of quartz-feldspathic composition alternating with mica-rich mafic bands that mark the compositional banding (Figs. 3A and 3B). Lenticular leucogranite veins are concordant with the mm- to cm-thick banding of the gneiss. Microscopically, this gneiss exhibits granoblastic bands of quartz, feldspar, and garnet, alternating with lepidoblastic bands of muscovite, biotite, and sillimanite (Figs. 3C and 3D). Cordierite is observed in both granoblastic and granolepidoblastic bands (Figs. 3E and 3F).

The pelitic paragneiss of the FH-21 outcrop is a gray gneiss with pink bands. The fine-grained and foliated appearance marks a subtle gneissic banding with concordant granitic lenses and biotite porphyroblasts (Figs. 4A and 4B). This gneiss shows tight folds and boudinated quartz veins. Microscopically, this rock exhibits a granolepidoblastic texture of muscovite and quartz with biotite porphyroblasts and granoblastic quartz lenses (Fig. 4C). These biotite porphyroblasts were rotated and are transversal and concordant with the rock foliation (Fig. 4D). Cordierite and garnet crystalloblasts are locally present (Figs. 4E and 4F). Classifying this rock as a cordierite-garnet-biotite-muscovite gneiss.

5.2 Mica schists

Mica schists and quartz-mica schists have been mapped as the predominant rocks of the Jacareacanga Group, although they rarely crop out as xenoliths, which are hosted in the orthogneisses and porphyroclastic granitoids of the Cuiú-Cuiú Complex (Ferreira et al., 2000; Melo et al., 1980).

In the Espírito Santo artisanal mine, located at the headwaters of the Parauari River (Fig. 2), mica schist (MV-58A) and quartz-mica schist (MV-58C) crop out. The saprolite of these schists is pink and ocher, while the fresh rock is light gray. Locally, quartz venules are mineralized with gold lattices concordant with the schistosity (Fig. 5A).

The Mica schist MV-58A is composed of lepidoblastic muscovite layers intercalated with subordinate granolepidoblastic quartz and feldspar layers. Both layers are impregnated with iron hydroxide ions along the schistosity (Fig. 5B). The quartz-mica schist MV-58C is composed of granolepidoblastic layers of quartz and feldspar, with subordinated biotite (Fig. 5C). The sigmoidal quartz and feldspar clasts of the matrix are contoured by biotite lamellae (Fig. 5D).

5.3 Amphibolites

Actinolite schists, talc-tremolite schists, and amphibolites, previously mapped by Ferreira et al. (2000) and Melo

et al. (1980), are interlayered with the mica schists of the Jacareacanga Group, and locally crop out as xenoliths hosted within the orthogneisses and porphyroclastic granitoids of the Cuiú-Cuiú Complex. The amphibolite of the MV-59 outcrop is close to the pelitic paragneiss FH-27 (Fig. 2), probably representing an amphibolite lens interlayered in the pelitic paragneiss.

The MV-59 amphibolite is a fine-grained, greenish-black, metamorphosed mafic rock characterized by tight folds in its foliation (Fig. 6A). Microscopically, MV-59 shows an alternation of hornblende-rich mafic levels and subordinate plagioclase-rich felsic levels (Fig. 6B). The mafic levels display nematoblastic arrangements of hornblende crystals (Fig. 6C), and the felsic levels exhibit polygonal granoblastic structures of plagioclase and subordinate hornblende (Fig. 6D).

6 LA-ICP-MS U-Pb ZIRCON DATING

Two samples of pelitic paragneisses (FH-21 and FH-27) from different outcrops and a mica schist (MV-58A) and quartz-mica schist (MV-58C) sample from the same outcrop were selected for LA-ICP-MS U-Pb zircon dating (Fig. 2).

6.1 Pelitic paragneiss FH-27

Pelitic paragneiss FH-27 contains elongated, euhedral prismatic crystals, with subordinate subhedral, sub-rounded, and rounded crystals. These zircons are transparent or translucent, ranging from colorless to yellow-brownish. CL images show well-defined oscillatory concentric zoning (Fig. 7), similar to those shown by Corfu et al. (2003) for igneous zircon crystals. Some crystals exhibit rounded and metamictized cores.

The paragneiss FH-27 zircon crystals yielded U contents between 2 and 157 ppm and Th/U ratios between 0.03 and 1.55 (Suppl. File 1). Despite most of the crystals yielded $^{207}\text{Pb}/^{206}\text{Pb}$ ages concordant by up to $100 \pm 10\%$, some presented high discordance ($> 10\%$) or were affected by U and Pb losses and plotted above and below the concordia curve (Fig. 8A).

In order to obtain a more robust dataset, previous results obtained by Vasquez et al. (2019) were added to our data (Suppl. File 2). The resulting histograms and relative probability curves highlight two populations of $^{207}\text{Pb}/^{206}\text{Pb}$ ages — one of 2021 Ma and another of 1970 Ma (Fig. 8B). The 2021 Ma population complies with the age cutoff of $^{207}\text{Pb}/^{206}\text{Pb} > 2000$ Ma adopted by Vasquez et al. (2019) (Fig. 8C), and is maintained using only our data (Fig. 8D). However, using only the crystals with superposition of $^{207}\text{Pb}/^{206}\text{Pb}$ ages, the diagrams show peaks at 2010 Ma and 2035 Ma (Fig. 8E). This may indicate that the $^{207}\text{Pb}/^{206}\text{Pb}$ age of 2021 Ma represents an average value of these two populations.

Other peaks in the relative probability curves indicate modest inputs from Rhyacian, Siderian, Neoproterozoic, and Mesoproterozoic zircon sources (Figs. 8B to 8E).

6.2 Pelitic paragneiss FH-21

Pelitic paragneiss FH-21 zircon crystals are either rounded or irregular, transparent or translucent, and brownish. CL images

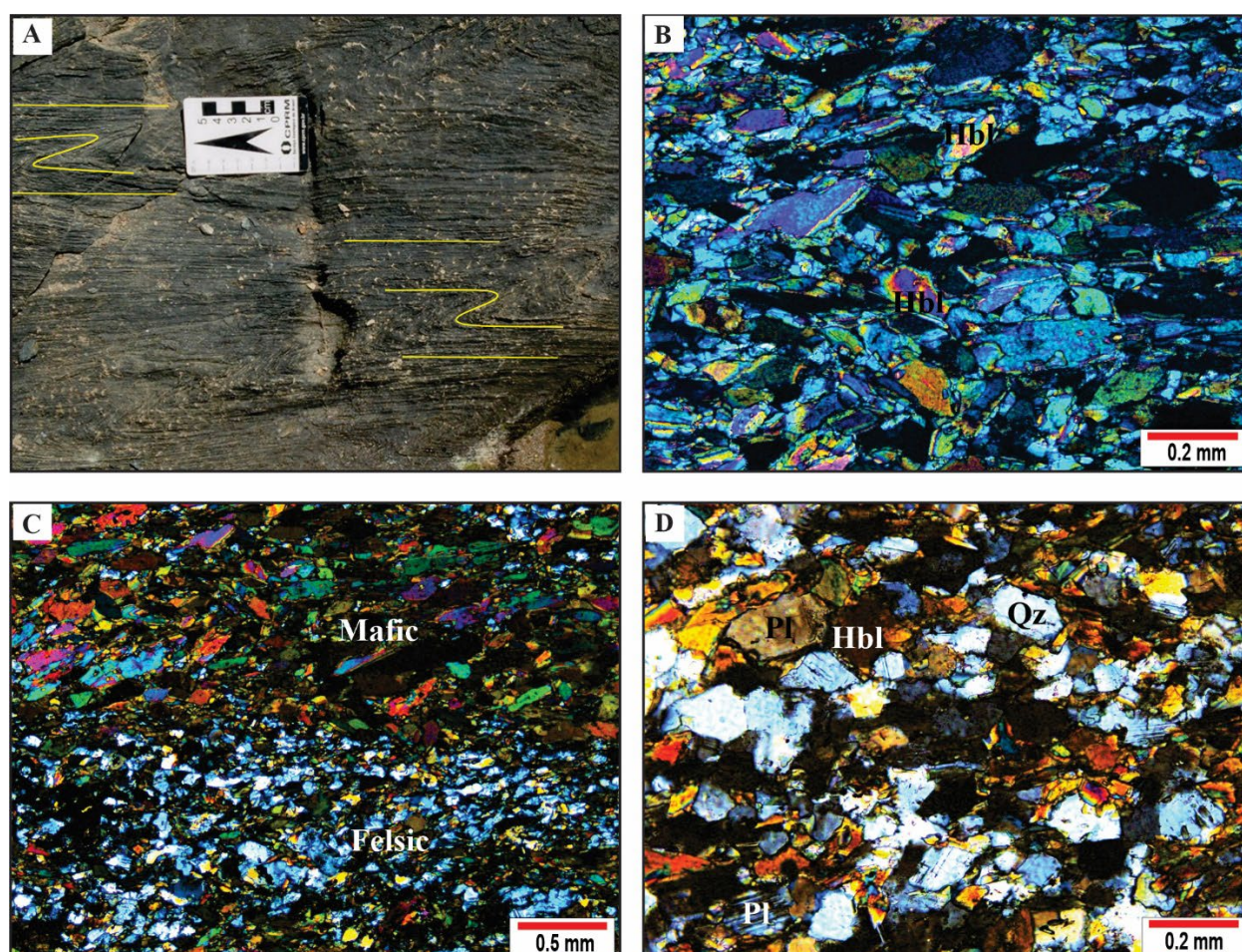


Figure 6. Structures and textures of amphibolite MV-59: (A) Tight folds in the amphibolite foliation; (B) Mafic band rich in amphibole and felsic band rich in plagioclase; (C) Nematoblastic texture of hornblende (Hbl) in the mafic band; (D) Polygonal granoblastic texture of plagioclase (Pl) and subordinate hornblende in the felsic level. Photomicrographs taken in polarized light.

indicate that igneous oscillatory zoning has been erased, with convoluted and sectoral zoning (Fig. 7) indicative of high-grade metamorphic recrystallization (Corfu et al., 2003). U contents and Th/U ratios in these zircon crystals range between 1 and 144 ppm and 0.06 to 1.39 respectively (Suppl. File 3). Additional LA-ICP-MS U-Pb isotopic data for sample FH-21 was taken from Vasquez et al. (2019) (Suppl. File 4). A few crystals plot above the concordia curve, exhibiting high errors (large ellipses) and high common lead (horizontal ellipses), marked by high ^{204}Pb contents (Fig. 9A).

Histograms and relative probability curves of the $^{207}\text{Pb}/^{206}\text{Pb}$ ages obtained in this study and by Vasquez et al. (2019) highlight populations with ages of 1993, 2042, and 2117 Ma (Fig. 9B). Disregarding ages < 2000 Ma, the 2042 Ma-old population stands out, and peripheral populations of 2074 and 2197 Ma appear (Fig. 9C). Applying this criterion only to our data, two peaks — one at 2008 Ma and another at 2039 Ma (Orosirian ages) — stand out, along with a Rhyacian population with a peak of 2117 Ma (Fig. 9D). The superposition treatment of the $^{207}\text{Pb}/^{206}\text{Pb}$ ages for all results > 2000 Ma reveals a bimodality for the Orosirian population with peaks at 2009 and 2050 Ma and a Rhyacian population of 2165 Ma (Fig. 9E).

Zircon sources with Rhyacian, Siderian, Neoproterozoic, and Paleoproterozoic $^{207}\text{Pb}/^{206}\text{Pb}$ ages were also identified in

pelitic paragneiss FH-21 (Figs. 9B to 9E). Peaks of different ages (2117, 2165, and 2197 Ma) mark the Rhyacian zircon sources. A peak of 2074 Ma is difficult to distinguish from the Orosirian population distribution curve (Fig. 9C). Subordinate contributions from Siderian, Neoproterozoic, and Paleoproterozoic sources were evident in the sediments that constituted this paragneiss.

6.3 MV-58 mica schists

Zircon crystals from mica schist MV-58A and quartz-mica schist MV-58C are euhedral, subhedral, and sub-rounded, transparent, colorless and brownish, with elongated, flattened prismatic habit. Most CL images show igneous oscillatory zoning in the crystals (Fig. 7). Some crystal cores present high luminescence (white color) that contrasts with less luminescent (gray) rims, indicating varying Th and U contents (Corfu et al., 2003). U contents and Th/U ratios range from 2 to 2,935 ppm and from 0.03 to 1.81 respectively (Suppl. File 5). A few crystals deviate significantly from the concordia curve, indicating high errors and high elevated common lead contents (Fig. 10A).

Histograms and relative probability curves of the $^{207}\text{Pb}/^{206}\text{Pb}$ ages obtained for mica schist MV-58A zircons reveal sources with a peak at 2055 Ma, followed by peaks at 2113 Ma and

2192 Ma (Fig. 10B). In quartz-mica schist MV-58C, a peak at 2034 Ma is distinguished, followed by a peak at 2121 Ma and subordinate peaks of Rhyacian ages (Fig. 10C). The 163 crystals of the two samples yield notable age peaks at 2056 Ma

and 2113 Ma and a subordinate peak at 2192 Ma (Fig. 10D). Restricting the analysis to ages > 2000 Ma, peaks of similar ages (2057, 2116, and 2193 Ma) are obtained (Fig. 10E), suggesting little influence of events occurring after the formation of these

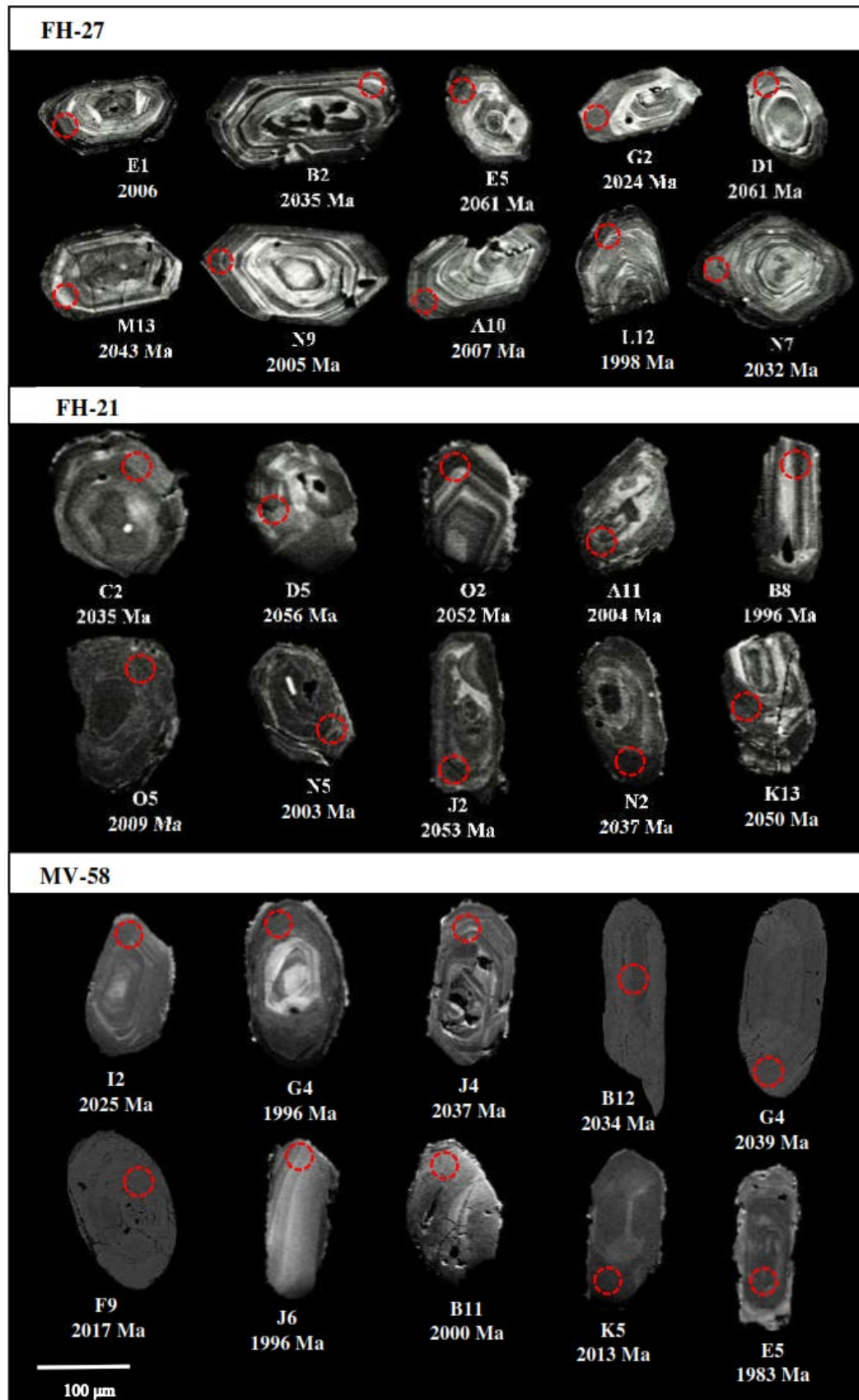


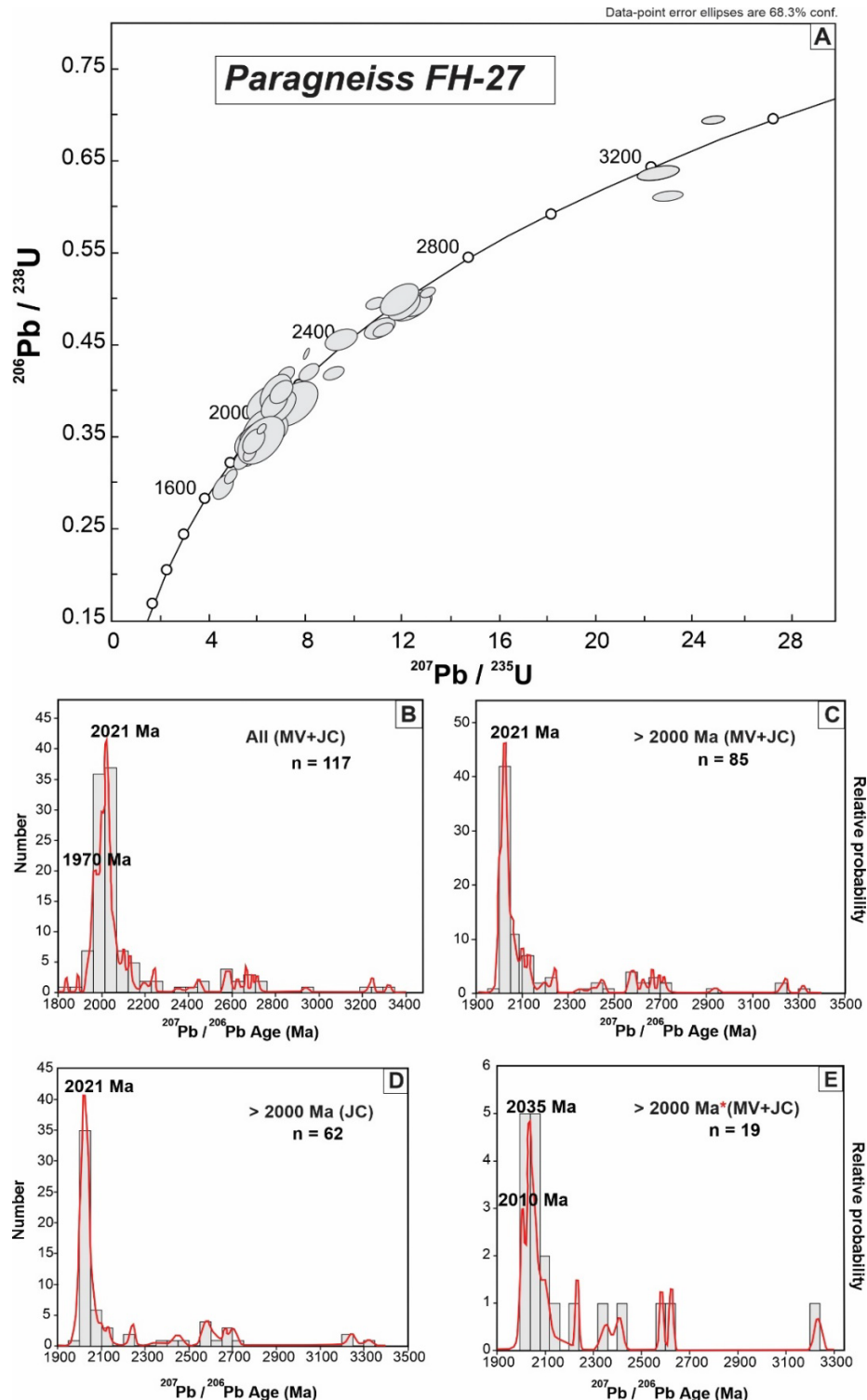
Figure 7. Representative cathodoluminescence images of detrital zircon crystals from two pelitic paragneisses (FH-21 and FH-27) and a mica schist (MV-58). The circles demarcate the spot locations (25 µm) and their respective $^{207}\text{Pb}/^{206}\text{Pb}$ ages by LA-ICP-MS.

mica schists. Applying the $^{207}\text{Pb}/^{206}\text{Pb}$ age superposition treatment to these data, a subtle peak appears at 2041 Ma, which is associated with the younger detrital source distribution curve. It is marked by the peak at 2064 Ma, followed by successive Rhyacian sources and subordinate Siderian, Neoproterozoic and Mesoproterozoic sources (Fig. 10F).

The peak at 2034 Ma (Fig. 10C) indicates that zircon sources of Orosirian ages contributed to the sediments that formed the mica schists, with major inputs from Rhyacian-age sources.

7 DISCUSSION

The metasedimentary and basic metavolcanic rocks of the Jacareacanga Group are the oldest rocks of the Tapajós Domain in the Tapajós-Parima Province and represent a Cuiú-Cuiú Arc basin (Santos et al., 2000, 2004). These rocks were formed during the Orosirian, when this magmatic arc was accreted. Contributions from older crustal sources are evident in these rocks, as the Cuiú-Cuiú Arc was accreted to an Archean craton (Santos et al., 2000; Tassinari, 1996; Tassinari & Macambira, 1999, 2004).

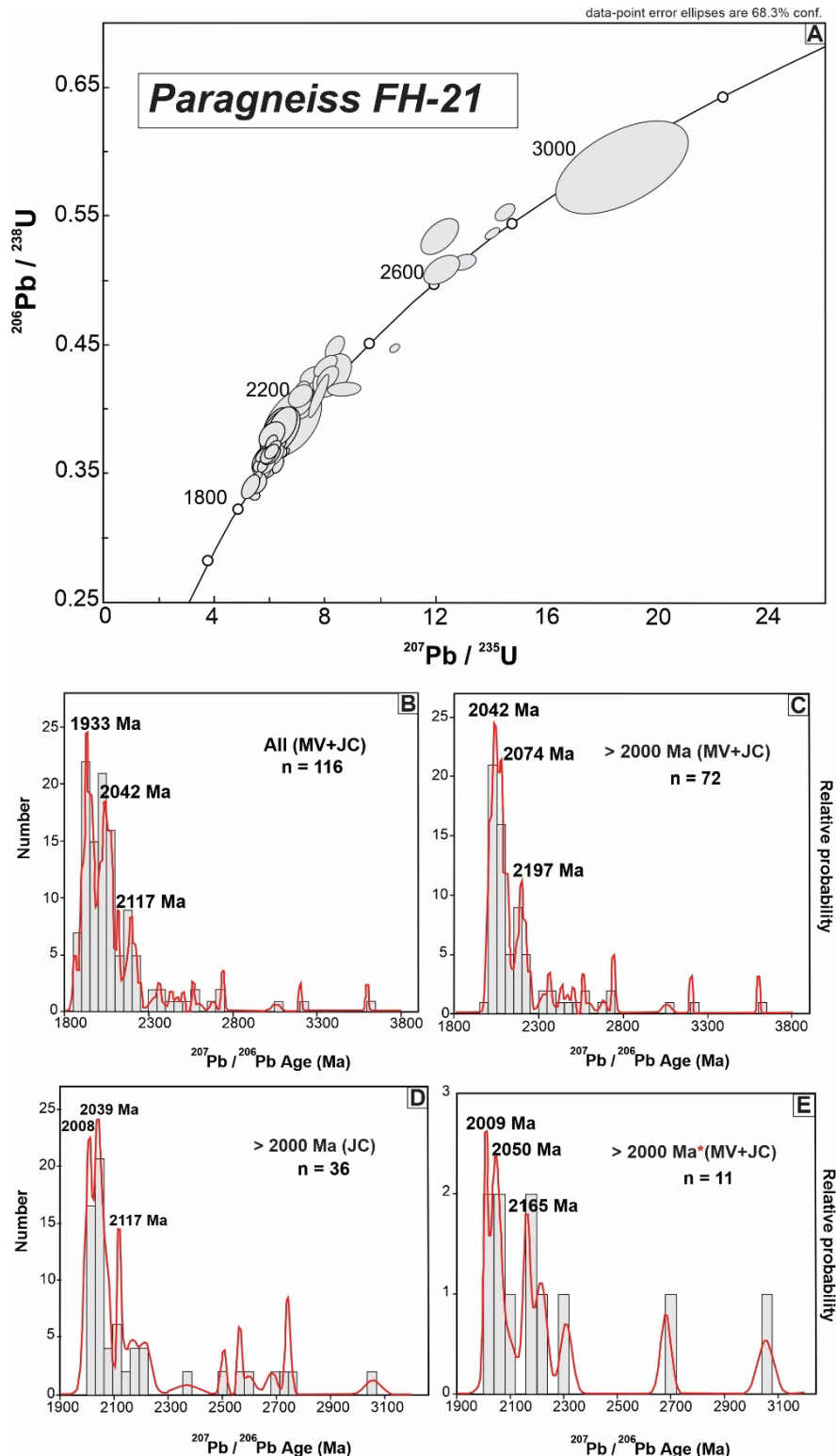


JC: our data; MV: data from Vasquez et al. (2019).

Figure 8. Diagrams of LA-ICP-MS U-Pb detrital zircon ages for pelitic paragneiss FH-27: (A) Concordia diagram; (B, C, D, E) Histograms and relative probability curves for $^{207}\text{Pb}/^{206}\text{Pb}$ ages of $100 \pm 10\%$ concordance. (B) All grains from this study and from Vasquez et al. (2019); (C) Zircon ages > 2000 Ma from this study and from Vasquez et al. (2019). (D) our data; (E) Zircon grains with superposition of age errors.

Detrital zircon ages have been obtained to help discriminate tectonic settings (Cawood et al., 2012; Gehrels, 2014; Von Eynatten & Dunkl, 2012). Previous studies of the Jacareacanga Group schists provided ages of *ca.* 2100 Ma and 2875 Ma (Santos et al., 2000) and of 2008 and 2034 Ma by the Pb-evaporation method (Almeida et al., 2001b). Despite restrictions on the number of dated crystals and on the adequacy of the method

applied, the 2008 and 2034 Ma ages obtained by Almeida et al. (2001b) are compatible with the ages expected for the sedimentary rocks associated with the Orosirian (2050-1998 Ma) Cuiú-Cuiú Magmatic Arc (Santos et al., 2004). Furthermore, the ages of *ca.* 2100 Ma and 2875 Ma may represent detrital zircons derived from the oldest crust of the craton bordered by this arc (Santos et al., 2000).



JC: our data; MV: data from Vasquez et al. (2019).

Figure 9. Diagrams of LA-ICP-MS U-Pb detrital zircon ages for pelitic paragneiss FH-21: (A) Concordia diagram; (B, C, D, E) Histograms and relative probability curves for $^{207}\text{Pb} / ^{206}\text{Pb}$ ages of $100 \pm 10\%$ concordance. (B) All grains from this study and from Vasquez et al. (2019); (C) Zircon ages > 2000 Ma from this study and from Vasquez et al. (2019). (D) our data; (E) Zircon grains with superposition of age errors.

The new LA-ICP-MS U-Pb zircon data obtained for four metasedimentary rock samples (two from pelitic paragneisses and two from mica schists) of the Jacareacanga Group, based on the treatment of $^{207}\text{Pb}/^{206}\text{Pb}$ ages, reveal significant contributions from Rhyacian zircon sources (peaks from 2056 to 2197 Ma), especially concerning samples FH-21, MV-58A, and MV-58C (Figs. 9 and 10). Siderian (2322 - 2453 Ma), Neoproterozoic (2510 - 2732 Ma), and Meso- to Paleoproterozoic (2878 - 3246 Ma) zircon sources were subordinate (Suppl. Material). Orosirian and Late Rhyacian populations, marked by peaks at 2021 Ma (sample FH-27), 2042 Ma (sample FH-21), and 2056 Ma (samples MV-58A and MV-58C),

represent a 2021 - 2056 Ma interval for sedimentation of the Jacareacanga Group.

Previous mapping campaigns of the Jacareacanga Group have only identified low-grade metamorphic rocks, such as mica schists, chlorite schists, actinolite schists, tremolite-talc schists, ferruginous metacherts, and quartzites (Melo et al., 1980). Locally, very low metamorphic grade meta-greywackes and metasiltites were mapped (Ferreira et al., 2000). Medium to high metamorphic grade rocks were only mapped as xenoliths hosted in granitoids and orthogneisses of the Cuiú-Cuiú Complex. Melo et al. (1980) described amphibolites and Ferreira et al. (2000) described sillimanite-cordierite-biotite

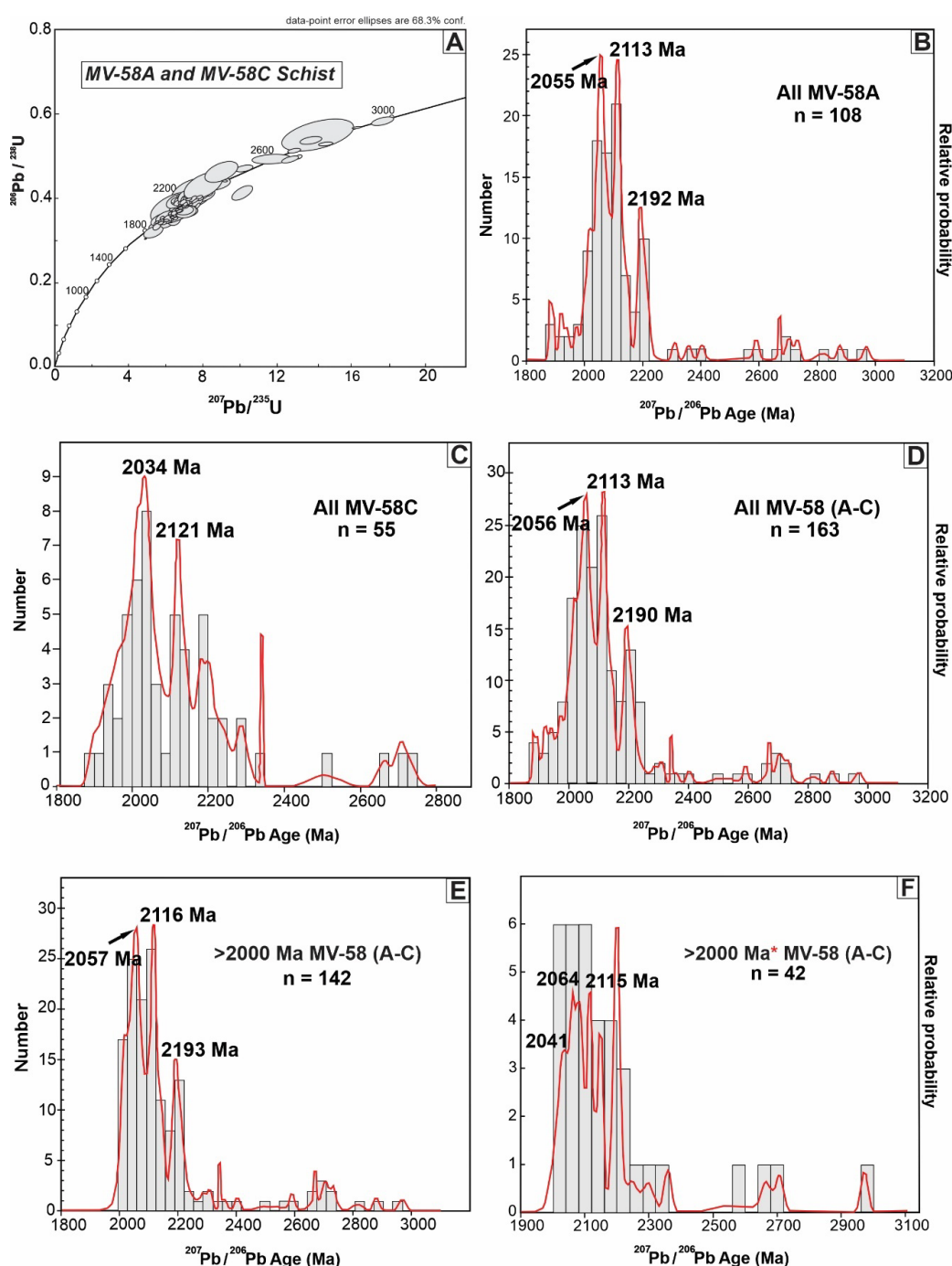


Figure 10. Diagrams of LA-ICP-MS U-Pb detrital zircon ages for the MV-58 mica schists: (A) Concordia diagram; (B, C, D, E, F) Histograms and relative probability curves for $^{207}\text{Pb}/^{206}\text{Pb}$ ages of $100 \pm 10\%$ concordance. (B) All grains from mica schist MV- 58A; (C) All grains from quartz-mica schist MV-58C. (D) All grains from sample MV-58A and sample MV-58C; (E) Grains of ages > 2000 Ma from both mica schists; (F) Zircon grains with superposition of age errors.

gneisses (pelitic paragneisses). In recent mapping campaigns, Vasquez et al. (2019, 2020) identified pelitic paragneisses (samples FH-21 and FH-27) and amphibolite (sample MV-59) in the eastern part of the main body of the Jacareacanga Group (Fig. 2). Intense mylonitic recrystallization caused by the transposition of earlier metamorphic foliation in pelitic paragneisses and intercalated amphibolite lenses (Figs. 4 and 6) likely led to their previous mapping as mica schists and actinolite schists.

In this study, the microtextures of polygonal granoblastic recrystallization and paragenesis with sillimanite, cordierite, garnet, and biotite in the pelitic paragneisses (Figs. 3 and 4), along with polygonal nematoblastic recrystallization of the amphibolite (Fig. 6), indicate that these rocks have reached medium- to high-grade metamorphic conditions, possibly close to low-pressure granulite facies conditions (Bucher & Grapes, 2011; Passchier & Trouw, 2005).

In the northwest part of the main body of the Jacareacanga Group (Espírito Santo mine), mica schists (sample MV-58A) and quartz-mica schists (sample MV-58C) do not show relicts of high-temperature granoblastic recrystallization microtextures (Fig. 5), comparable to the polygonal granoblastic texture of *ca.* 500°C (Passchier & Trouw, 2005). In addition, these schists do not present the paragenesis (garnet, sillimanite, cordierite) typical of medium to high metamorphic grade pelitic rocks.

The high-grade metamorphic conditions are reinforced by the occurrence of cordierite-garnet-muscovite granite (peraluminous granite) lenses that crosscut pelitic paragneiss FH-27 (Figs. 3A and 3B). U-Pb zircon dating of this peraluminous granite yielded an age of 1956 ± 27 Ma, interpreted as the crystallization age of a probable anatexis product of pelitic paragneisses (Vasquez et al., 2019). Furthermore, these authors identified a zircon population of 1890 ± 34 Ma of age in the pelitic paragneiss FH-21, correlatable with the granitoids of the Tropas Suite or of the Parauari Suite that intruded the main body of the Jacareacanga Group (Fig. 2). Based on this evidence, Vasquez et al. (2019) proposed that events younger than 2000 Ma affected the rocks of this unit, supporting the criterion adopted in this study of restricting data treatment to U-Pb zircon ages older than 2000 Ma.

The 2021 Ma-old zircon population of the pelitic paragneiss FH-27 (Fig. 8C) shows a peak at 2010 Ma and another at 2035 Ma, when applying the superposition criterion (Fig. 8E). This bimodality of the Orosirian population identifies pulses in the zircon sources compatible with the ages of the 2033 to 2005 Ma-old granitoids of the Cuiú-Cuiú Complex (Santos et al., 2004; Vasquez et al., 2017) and the 2009 to 2020 Ma-old felsic volcanic rocks of the Comandante Arara Formation (Vasquez et al., 2017). The peak at 2042 Ma identified in the pelitic paragneiss FH-21 data is followed by Rhyacian peaks at 2074 Ma and 2197 Ma (Fig. 9C). The bimodality of the Orosirian population (Fig. 9D) is accentuated when applying the superposition criterion (Fig. 9E).

Mica schist samples MV-58A and MV-58C were analyzed together due to their similar outcrop origins, *e.g.* quartz-mica schist MV-58C is richer in quartz than MV-58A. The detrital zircon crystals older than 2000 Ma show a main peak at 2057

Ma, followed by peaks at 2116 Ma and 2193 Ma (Fig. 10E). The superposition criterion reveals a peak at 2041 Ma, subordinate to the main peak at 2064 Ma (Fig. 10F). The distribution curves of detrital zircon populations in the mica schists suggest a significant contribution from Rhyacian zircon sources (Figs. 10E and 10F). According to these results, the input from Rhyacian zircon sources is more significant to the mica schists than to the pelitic paragneisses (Figs. 8D and 8E).

The significant contribution of Rhyacian sources may have attenuated the contribution of Orosirian sources derived from the rocks of the Cuiú-Cuiú Arc to the mica schists of the northwest part of the Jacareacanga Group. On the other hand, the contribution from Rhyacian sources and sources of older ages to the pelitic paragneiss FH-21 was weaker (Figs. 9C to 9E), indicating that its primary source was the Cuiú-Cuiú Arc igneous rocks.

It was not possible to properly date amphibolite MV-59, which marks the basaltic volcanism intercalated with the pelitic sediments represented by the pelitic paragneisses (samples FH-21 and FH-27). Only three crystals were dated, one of them yielding a $^{207}\text{Pb}/^{206}\text{Pb}$ age of 2059 ± 25 Ma, which is close to the ages of the sediments that formed the paragneisses.

The immature pelitic sedimentation is marked by pelitic paragneisses (samples FH-21 and FH-27), and possibly the mica schists (samples MV-58A and MV-58C), with intercalations of ocean floor basaltic lavas represented by the actinolite schists, talc-tremolite schists, and amphibolites mapped by Ferreira et al. (2000) and Melo et al. (1980). This volcano-sedimentary sequence represents turbiditic sedimentation in an oceanic trench basin of the Cuiú-Cuiú Arc (Santos et al., 2000, 2004). According to our LA ICP-MS U-Pb data, the pelitic sediments were deposited in the Jacareacanga Basin between 2057 and 2021 Ma. The peraluminous granites represent a probable anatexis of these metapelitic rocks, which underwent high-grade metamorphism at 1956 ± 27 Ma (Vasquez et al., 2019).

8 CONCLUSIONS

Based on data obtained from Geological Survey of Brazil mapping campaigns in the Tapajós Domain (Mineral Province of Tapajós) within the Tapajós-Parima Province, combined with petrographic studies and LA-ICP-MS U-Pb zircon geochronology applied to metasedimentary rocks of the Jacareacanga Group, it was possible to not only investigate provenance and constrain the maximum sedimentation age.

The pelitic paragneisses in the eastern part of the main body of the Jacareacanga Group comprise sillimanite-cordierite-garnet-biotite gneisses (samples FH-21 and FH-27), intercalated with amphibolite lenses (sample MV-59). High-grade metamorphism with anatexis of indicated by the presence of peraluminous granites veins. In contrast, mica schists (samples MV-58A and MV-58C) from the northwestern part of the Jacareacanga Group resulted from low-grade metamorphism to the greenschist facies, indicating increasing metamorphic conditions from west to east.

Previous dating of the peraluminous granite veins cross-cutting the pelitic paragneisses yielded ages of *ca.* 1960 Ma. Likewise, granitoid intrusions in mica schists and paragneisses were dated *ca.* 1890 Ma. Thus, detrital zircon data were constrained to $^{207}\text{Pb}/^{206}\text{Pb}$ ages > 2000 Ma, in order to define provenance. To eliminate spurious data, a concordance of $100 \pm 10\%$ was adopted in relation to the apparent $^{207}\text{Pb}/^{206}\text{Pb}$ and $^{207}\text{Pb}/^{238}\text{U}$ ages in order to better evaluate the relative probability curves obtained for each zircon population. Furthermore, by applying the superposition of $^{207}\text{Pb}/^{206}\text{Pb}$, $^{206}\text{Pb}/^{238}\text{Pb}$, and $^{207}\text{U}/^{235}\text{Pb}$ ages to obtain these curves, it was possible to verify polymodalities of the main Orosirian and Rhyacian zircon populations of the paraderived rocks of the Jacareacanga Group.

The geochronological data obtained for the pelitic paragneisses and mica schists point to sources with ages from 2021 to 2057 Ma, which represent the maximum age of sedimentation of the sediments that originated the Jacareacanga Group metasedimentary rocks.

The Orosirian ages of deposition of the original pelitic sediments reinforce the correlation of the Jacareacanga Basin with the Cuiú-Cuiú Arc. The occurrence of zircon populations of Rhyacian ages and subordinate Siderian to Archean ages attests that it was a continental margin magmatic arc.

ACKNOWLEDGEMENTS

We thank the Geological Survey of Brazil for providing the rock samples analyzed in this study and for making available the LAMIN-BE facilities for samples preparation, petrographic and SEM studies. We also thank the Universidade Federal do Pará (UFPA), in particular the Post-Graduation Program in Geology and Geochemistry (PPGG) and the Laboratory of Isotopic Geology (Para-Iso), for the support to the geochronological studies. The first author is grateful to CAPES for the M. Sc. scholarship (Process 88887.351816/2019-00).

ARTICLE INFORMATION

Manuscript ID: e20240021. Received on: 25 JUNE 2024. Approved on: 2 DEC 2024.

How to cite: Cardozo, J. A. O., Vasquez, M. L., & Toro, M. A. G. (2025). LA-ICP-MS U-Pb zircon dating of rocks of the Jacareacanga Group, Tapajós Domain, Amazon Craton, Brazil. *Brazilian Journal of Geology*, 55, e20240021. <https://doi.org/10.1590/2317-4889202520240021>

JAOC: Investigation, wrote the manuscript, prepared the samples for analysis, formal analysis, acquired and treated geochronological data, prepared figures and tables, discussed geochronology and petrography data, corrected the manuscript. MLV: Validation, Supervision, mapped the geology, selected samples, structural support for sample preparation, discussed petrology, wrote and improved the manuscript, discussed geochronology data. MAG: Validation, Supervision, acquired and treated geochronological data, discussed geochronology data, writing - review and editing and funding acquisition.

Conflict of interest: nothing to declare.

REFERENCES

- Almeida, M. E., Brito, M. F. L., Ferreira, A. L., & Monteiro, M. A. S. (2000). *Geologia e recursos minerais da Folha Vila Mamãe Anã - SB.21-V-D: Estados do Amazonas e Pará: Escala 1:250.000*. CPRM. Programa de Levantamentos Geológicos Básicos do Brasil (PLGB). Projeto Especial Província Mineral do Tapajós (PROMIN Tapajós). Retrieved from <https://rigeo.cprm.gov.br/handle/doc/2567>
- Almeida, M. E., Ferreira, A. L., Brito, M. F. L., & Monteiro, M. A. S. (2001a). Proposta de evolução tectono-estrutural da Província Tapajós com base na geologia das folhas Vila Mamãe Anã e Jacareacanga (1:250.000), região limite dos Estados do Amazonas e Pará. In: N. J. Reis & M. A. S. Monteiro (coords.). *Contribuições à geologia da Amazônia* (Vol. 2, pp. 57-112). SBG. Retrieved from <http://arquivos.sbg-no.org.br/BASES/CGA%202.pdf>
- Almeida, M. E., Ferreira, A. L., Macambira, M. J. B., & Sachtet, C. R. (2001b). Time constraint based on zircon dating for the Jacareacanga Group (Tapajós Province, Amazon Craton, Brazil). In: 3^o *South American Symposium on Isotope Geology*, Pucon, Chile. Retrieved from <https://www.researchgate.net/publication/318018915>
- Andersen, T. (2005). Detrital zircons as tracers of sedimentary provenance: limiting conditions from statistics and numerical simulation. *Chemical Geology*, 216(3-4), 249-270. <https://doi.org/10.1016/j.chemgeo.2004.11.013>
- Bahia, R. B. C., & Quadros, M. L. E. S. (2000). *Geologia e recursos minerais da Folha Caracol SB.21-X-C: Estados do Pará e Amazonas, Escala 1:250.000*. Companhia de Pesquisas de Recursos Minerais. Retrieved from <http://rigeo.cprm.gov.br/jspui/handle/doc/3068>
- Bizinella, G. A., Santiago, A. F., Santos, A., Borges, F. R., Souza, F. J. C., Godoy, H. K., Yamaguti, H. S., Oliveira, J. R., & Oliveira, L. R. (1980). *Projeto Tapajós-Sucunduri: Relatório Final*. DNPM/CPRM. Retrieved from <http://rigeo.cprm.gov.br/jspui/handle/doc/6686>
- Borgo, A., Biondi, J. C., Chauvet, A., Bruguier, O., Monie, P., Baker, T., & Mortensen, J. (2017). Geochronological, geochemical and petrographic constraints on the Paleoproterozoic Tocantinzinho gold deposit (Tapajós Gold Province, Amazonian Craton-Brazil): Implications for timing, regional evolution and deformation style of its host rocks. *Journal of South American Earth Sciences*, 75, 92-115. <https://doi.org/10.1016/j.jsames.2017.02.003>
- Bucher, K., & Grapes, R. (2011). *Petrogenesis of metamorphic rocks*. Springer.
- Cassini, L. V., Moyen, J. F., & Juliani, C. (2020). Orosirian magmatism in the Tapajós Mineral Province (Amazonian Craton): The missing link to understand the onset of Paleoproterozoic tectonics. *Lithos*, 356-357, 105350. <https://doi.org/10.1016/j.lithos.2019.105350>
- Cawood, P. A., Hawkesworth, C. J., & Dhuime, B. (2012). Detrital zircon record and tectonic setting. *Geology*, 40(10), 875-878. <https://doi.org/10.1130/G32945.1>
- Chemale Jr., F., Kawashita, K., Dussin, I. A., Ávila, J. N., Justino, D., & Bertotti, A. L. (2012). U-Pb zircon *in situ* dating with LA-MC-ICP-MS using a mixed detector configuration. *Anais da Academia Brasileira de Ciências*, 84(2), 275-295. <https://doi.org/10.1590/S0001-37652012005000032>
- Corfu, F., Hanchar, J. M., Hoskin, P. W. O., & Kinny, P. (2003). Atlas of zircon textures. In: J. M. Hanchar & P. W. O. Hoskin (Eds.), *Zircon: reviews in mineralogy and geochemistry* (Vol. 53, pp. 469-500). Mineralogical Society of America.
- Coutinho, M. G. N. (2008). Evolução tectono-geológica e modelo de mineralização de ouro. In: M. G. N. Coutinho (Ed.), *Província Mineral do Tapajós: Geologia, metalogenia e mapa provisional para ouro em SIG* (pp. 251-262). CPRM. Retrieved from <https://rigeo.cprm.gov.br/handle/doc/1208>

- Coutinho, M. G. N., Souza, E. C., Liverton, T., Guimarães, M. T., & Walsh, J. N. (2008). Petrologia e geoquímica das rochas hospedeiras. In: M. M. G. N. Coutinho (Ed.), *Provincia Mineral do Tapajós: geologia, metalogenia e mapa provisional para ouro em SIG* (pp. 251-262). CPRM. Retrieved from <https://rigeo.cprm.gov.br/handle/doc/1208>
- Ferreira, A. L., Almeida, M. E., Brito, M. F. L., & Monteiro, M. A. S. (2000). *Geologia e recursos minerais da Folha Jacareacanga - SB.21-Y-B: Estados do Amazonas e Pará. Escala 1:250.000*. CPRM. Programa Levantamentos Geológicos Básicos do Brasil (PLGB). Projeto Especial Provincia Mineral do Tapajós (PROMIN Tapajós). Retrieved from <https://rigeo.cprm.gov.br/handle/doc/5671>
- Gehrels, G. (2014). Detrital zircon U-Pb geochronology applied to tectonics. *Annual Review of Earth and Planetary Sciences*, 42, 127-149. <https://doi.org/10.1146/annurev-earth-050212-124012>.
- Guimarães, S. B., Klein, E. L., Lisboa, C. L., Souza, S. M. D., Castro, J. M. R. D., Queiroz, J. D., & Lima, R. G. C. (2015). *Metalogenia das províncias minerais do Brasil: área sudeste do Tapajós. Estado do Pará*. CPRM. Retrieved from http://dspace.cprm.gov.br/bitstream/doc/16601/1/Irm_PMB_03_Tapajós.pdf
- Jackson, S. E., Pearson, N. J., Griffin, W. L., & Belousova, E. A. (2004). The application of laser ablation inductively coupled plasma-mass spectrometry to in situ U-Pb zircon geochronology. *Chemical Geology*, 211(1-2), 47-69. <https://doi.org/10.1016/j.chemgeo.2004.06.017>
- Klein, E. L., & Vasquez, M. L. (2000). *Geologia e recursos minerais da Folha Vila Riozinho - SB.21-Z-A: Estados do Amazonas e Pará: Escala 1:250.000*. CPRM. Programa Levantamentos Geológicos Básicos do Brasil (PLGB). Projeto Especial Provincia Mineral do Tapajós (PROMIN - Tapajós). Retrieved from <https://rigeo.cprm.gov.br/handle/doc/2574>
- Klein, E. L., Almeida, M. E., Vasquez, M. L., Bahia, R. B. C., Quadros, M. L. E. S., & Ferreira, A. L. (2001). *Geologia e recursos minerais da Provincia Mineral do Tapajós. Folhas SB.21-V-D, SB.21-Y-B, SB.21-X-C e SB.21-Z-C, Estados do Pará e Amazonas*. CPRM. Programa Levantamentos Geológicos Básicos do Brasil. Projeto Especial Provincia Mineral do Tapajós (PROMIN - Tapajós). Retrieved from <https://rigeo.cprm.gov.br/handle/doc/5050>
- Lamarão, C. N., Dall'Agnol, R., Lafon, J. M., & Lima, E. F. (2002). Geology, geochemistry, and Pb-Pb zircon geochronology of the Paleoproterozoic magmatism of Vila Riozinho, Tapajós Gold Province, Amazonian Craton, Brazil. *Precambrian Research*, 119, 189-223. [https://doi.org/10.1016/S0301-9268\(02\)00123-7](https://doi.org/10.1016/S0301-9268(02)00123-7)
- Lamarão, C. N., Dall'Agnol, R., & Pimentel, M. M. (2005). Nd isotopic composition of Paleoproterozoic volcanic and granitoid rocks of Vila Riozinho: implications for the crustal evolution of the Tapajós gold province, Amazon craton. *Journal of South American Earth Science*, 18, 277-292. <https://doi.org/10.1016/j.jsames.2004.11.005>
- Ludwig, K. R. (2012). *User's manual for Isoplot 3.75: a geochronological toolkit for Microsoft Excel*. Berkeley Geochronology Center.
- Melo, A. F. F., Andrade, A. F., Yamaguti, H. S., Oliveira, J. R., Carmona, J. R. M., D'Antona, R. J. G., & Lopes, R. C. (1980). *Projeto Tapajós-Sucunduri: Relatório Final*. CPRM/DNPM. Retrieved from <https://rigeo.cprm.gov.br/handle/doc/6686>
- Milhomem Neto, J. M., Lafon, J. M., Galarza, M. A., & Moura, C. A. V. (2017). U-Pb em zircão por LA-MC-ICP-MS no laboratório Pará-Iso (UFPA): metodologia e aplicação na porção sudoeste do Escudo das Guianas. In: N. J. Reis & M. A. S. Monteiro (Coords.), *Contribuições à geologia da Amazônia* (Vol. 10, p. 333-346).
- Passchier, C. W., & Trouw, R. A. J. (2005). *Microtectonics* (2ª ed.). Springer.
- Pessoa, M. R., Santiago, A. F., Andrade, A. F., Nascimento, J. O., Santos, J. O. S., Oliveira, J. R., Lopes, R. C., & Prazeres, W. V. (1977). *Projeto Jamanxim. Relatório Final* (3 vol.). DNPM / CPRM. Retrieved from <https://rigeo.cprm.gov.br/handle/doc/9404>
- Santos, J. O. S. (2003). Geotectônica dos Escudos das Guianas e Brasil - Central. In: L. A. Bizzi, C. Schobbenhaus, R. M. Vidotti & J. H. Gonçalves (Eds.), *Geologia, tectônica e recursos minerais do Brasil* (pp. 169-226). CPRM.
- Santos, J. O. S., Groves, D. I., Hartmann, L. A., McNaughton, N. J., & Moura, M. B. (2001). Gold deposits of the Tapajós and Alta Floresta domains, Tapajós-Parima orogenic belt, Amazon Craton, Brazil. *Mineralium Deposita*, 36, 278-299. <https://doi.org/10.1007/s001260100172>
- Santos, J. O. S., Hartmann, L. A., Gaudette, H. E., Groves, D. I., McNaughton, N. J., & Fletcher, I. R. (2000). A new understanding of the provinces of the Amazon Craton based on integration of field mapping and U-Pb and Sm-Nd geochronology. *Gondwana Research*, 3(4), 453-488. [https://doi.org/10.1016/S1342-937X\(05\)70755-3](https://doi.org/10.1016/S1342-937X(05)70755-3)
- Santos, J. O. S., Van Breemen, O. T., Groves, D. I., Hartmann, L. A., Almeida, M. E., McNaughton, N. J., & Fletcher, I. R. (2004). Timing and evolution of multiple Paleoproterozoic magmatic arcs in the Tapajós Domain, Amazon Craton: Constraints from SHRIMP and TIMS zircon, baddeleyite and titanite U-Pb geochronology. *Precambrian Research*, 131, 73-109. <https://doi.org/10.1016/j.precamres.2004.01.002>
- Santos, M. M., Lana, C., Scholz, R., Buick, I., Schmitz, M. D., Kamo, S. L., Gerdes, A., Corfu, F., Tapster, S., Lancaster, S. P., Storey, C. D., Basei, M. A. S., Tohver, E., Alkmin, A., Nalini, H., Krambrock, K., Fantini, C., & Wiedenbeck, M. (2017). A new appraisal of Sri Lankan BB zircon as a reference material for LA-ICP-MS U-Pb geochronology and Lu-Hf isotope tracing. *Geostandards and Geoanalytical Research*, 41(3), 335-358. <https://doi.org/10.1111/ggr.12167>
- Santos, R. A., & Coutinho, M. G. N. (2008). Geologia estrutural. In: M. G. N. Coutinho (Ed.), *Provincia mineral do Tapajós: geologia, metalogenia e mapa provisional para ouro em SIG* (pp. 97-135). CPRM. Retrieved from <https://rigeo.cprm.gov.br/handle/doc/1208>
- Sato, K., & Tassinari, C. C. G. (1997). Principais eventos de acreção continental do Cráton Amazônico baseados em idade-modelos Sm-Nd, calculadas em evoluções de estágio único e estágio duplo. In: M. L. C. Costa & R. S. Angélica (Eds.), *Contribuições à geologia da Amazônia* (Vol. 1, pp. 91-142). FINEP/SBG.
- Tassinari, C. C. G. (1996). *O mapa geocronológico do Cráton Amazônico no Brasil: revisão dos dados isotópicos* (PhD Thesis, Instituto de Geociências, Universidade de São Paulo). <https://doi.org/10.11606/T.44.2013.tde-22082013-163642>
- Tassinari, C. C. G., & Macambira, M. J. B. (1999). Geochronological provinces of the Amazonian Craton. *Episodes*, 22(3), 174-182. <https://doi.org/10.18814/epiugs/1999/v22i3/004>
- Tassinari, C. C. G., & Macambira, M. J. B. (2004). A evolução tectônica do Cráton Amazônico. In: V. Mantesso Neto, A. Bartorelli, C. D. R. Carneiro & B. B. B. Neves (Eds.), *Geologia do Continente Sul-Americano: evolução da obra de Fernando Flávio Marques de Almeida* (pp. 471-485). Beca.
- Vasquez, M. L., & Klein, E. L. (2000). *Geologia e recursos minerais da Folha Rio Novo - SB.21-ZC: Estados do Amazonas e Pará: Escala 1:250.000*. CPRM. Programa de Levantamentos Geológicos Básicos do Brasil (PLGB). Projeto Especial Provincia Mineral do Tapajós (PROMIN - Tapajós). Retrieved from <https://rigeo.cprm.gov.br/handle/doc/8514>
- Vasquez, M. L., Castro, J. M. R., Chaves, C. L., Costa Neto, M. C., & Cruz, V. L. (2020). *Mapa de integração geológico-geofísica da ARIM Tapajós na escala 1:500.000*. Projeto Evolução Crustal e Metalogênese da Provincia Mineral do Tapajós. CPRM. Retrieved from <https://rigeo.cprm.gov.br/xmlui/handle/doc/18638>
- Vasquez, M. L., Chaves, C. L., Moura, E. L., & Oliveira, J. K. M. (2017). *Geologia e recursos Minerais das Folhas São Domingos - SB.21-Z-A-II e Jardim do Ouro - SB.21-Z-A-III, Estado do Pará, Escala: 1:100.000*. CPRM. Programa Geologia do Brasil (PGB). Integração e Difusão de Dados da Geologia do Brasil. Retrieved from <https://rigeo.cprm.gov.br/handle/doc/17997>
- Vasquez, M. L., Pinheiros, F. G. R., Rodrigues, J. B., Tavares, F. M., Chaves, C. L., & Faraco, M. T. L. (2019). Idades U-Pb por LA-ICP-MS em zircão das rochas do Grupo Jacareacanga, sudoeste do Domínio Tapajós. In: 16º *Simpósio de Geologia da Amazônia*. SBG. Retrieved from <http://www.sbggeo.org.br/home/pages/44>
- Vasquez, M. L., Ricci, P. S. F., & Klein, E. L. (2002). Granitoides pós-colisionais da porção leste da Provincia Tapajós. In: E. L. Klein, M. L. Vasquez & L. T. Rosa-Costa (Eds.), *Contribuições à geologia da Amazônia* (Vol. 3, pp. 67-84). SBG. Retrieved from <http://arquivos.sbgno.org.br/BASES/CGA%203.pdf>
- Vasquez, M. L., Rosa-Costa, L. T., Silva, C. M. G., & Klein, E. L. (2008). Compartimentação tectônica. In: M. L. Vasquez & L. T. Rosa Costa (Eds.), *Geologia e recursos minerais do Estado do Pará: Sistema de Informações Geográficas - SIG: texto explicativo do mapa geológico e tectônico e de recursos minerais do Estado do Pará. Escala 1:1.000.000* (pp. 39-112). CPRM. Retrieved from <https://rigeo.cprm.gov.br/handle/doc/10443>
- Vermeesch, P. (2004). How many grains are needed for a provenance study? *Earth and Planetary Science Letters*, 224, 441-451. <https://doi.org/10.1016/j.epsl.2004.05.037>
- Von Eynatten, H., & Dunkl, I. (2012). Assessing the sediment factory: the role of single grain analysis. *Earth-Science Reviews*, 115(1-2), 97-120. <https://doi.org/10.1016/j.earscirev.2012.08.001>